Earth and Planetary Science Letters 290 (2010) 375–390

Contents lists available at ScienceDirect

Earth and Planetary Science Letters

journal homepage: www.elsevier.com/locate/epsl

Placing limits on channel flow: Insights from the Bhutan Himalaya

Sean Long *, Nadine McQuarrie

Department of Geosciences, Princeton University, Princeton, NJ 08544, USA

ARTICLE INFO

Article history:
Received 28 August 2009
Received in revised form 13 December 2009
Accepted 16 December 2009
Available online 13 January 2010

Editor: T.M. Harrison

Keywords:
Himalayas
Bhutan
channel flow
strain
kinematics
U–Pb dating

ABSTRACT

Along the majority of the Himalayan orogenic belt, high-grade metamorphic rocks of the Greater Himalaya (GH) are separated from lower-grade metasedimentary rocks by two shear zones, the basal, top-to-the-south Main Central Thrust (MCT), and the upper, top-to-the-north South Tibetan Detachment (STD). Seemingly pervasive ductile deformation within GH rocks and a lack of exposed hanging wall or footwall cut-offs for the MCT and STD have permitted models that predict 100's of km of coeval displacement on both structures, extruding the GH section via gravitational loading from Tibet and focused erosion along the Himalayan topographic front. We present new mapping, stratigraphic columns, mineral assemblages, U/Pb zircon ages, and a suite of structural data from GH and Tethyan Himalayan (TH) rocks in eastern and central Bhutan. Our observations highlight significant, ~250–300 °C along-strike changes in the deformation temperature conditions recorded by GH rocks. In eastern Bhutan, TH rocks are separated from GH rocks displaying ubiquitous partial melt textures by a top-to-the-north sense shear zone correlated with the STD. However, in central Bhutan, limited partial melt textures are only present near the base of the GH section, a biotite–muscovite–garnet mineral assemblage persists from 0.2 to 3 km above the MCT through TH rocks, and distinct lithologies interfinger at the GH–TH contact, which suggests that TH strata are in depositional contact above GH strata. The same strata exposed on both sides of the STD limits slip along this structure to ~20 km. Thin-section scale top-to-the-south shear is focused in a 2–3 km-thick zone above the MCT while the overlying ~11 km-thick section displays top-to-the-north shear, suggesting asymmetric channel behavior. Strained quartz grains allow us to quantify ~23–34 km of top-to-the-north shear. Our data suggest that the GH–TH section in central Bhutan acted as a cool, viscous, low-displacement channel, and when compared to sections in eastern Bhutan highlights dramatic changes in temperature conditions, viscosity and possibly displacement along strike. However, we suggest that the erosion rates needed to remove low-viscosity material limit channel flow even in regions containing significant partial melt, and that the magnitude of channel flow is small compared to the total mass balance of the system.

© 2009 Elsevier B.V. All rights reserved.

1. Introduction

Since the recognition of potential crustal melt under the Tibetan plateau by the INDEPTH project (Nelson et al., 1996), and the development of numerical models which suggest southward extrusion of weak crust driven by gravitational potential energy of the Tibetan plateau and focused erosion along the topographic front (Beaumont et al., 2001), an increasingly polarized debate has taken place over the viability of channel flow between the MCT and the STD. The debate has focused on multiple aspects, including the fundamental definition of a "channel," the role of partial melt, the provenance of channel material, specific P–T requirements for flow, predicted versus observed exhumation rates, and the timing of flow, among others (e.g. Grujic, 2006; Harrison, 2006; Hollister and Grujic, 2006; Robinson and Pearson, 2006; Harris, 2007; Kohn, 2008). Many recent Himalayan studies present concise arguments both for and against channel flow on the basis of geologic observations (Grujic et al., 2002; Robinson and Pearson, 2006; Robinson et al., 2006; Searle et al., 2006; Harrison, 2006; Hollister and Grujic, 2006; Kohn, 2008).

Channel flow is the process in which an applied pressure gradient induces flow of less viscous material bound above and below by more viscous or rigid material, producing the highest material transport velocities in the center, and opposite vorticity at the top and bottom of the channel (Poiseuille flow or 'pipe' flow of Turcotte and Schubert (2002); see also summary in Grujic (2006)). Under this definition, channel flow is distinguished from the case of distributed shear only in the direction of transport, which is common in many large, ductile thrusts. In geologic studies, a channel would be defined by a penetratively-deformed section of rock with opposite sense of distributed shear in the upper half and lower half of the column, creating the largest displacement in the center. Although *in situ* partial melting is interpreted as the most likely strength-lowering mechanism needed to initiate and sustain channel flow (Grujic, 2006; Hollister and Grujic, 2006; Harris, 2007), a channel flow profile of distributed shear may also

* Corresponding author. Tel.: +1 609 258 9836; fax: +1 609 258 1274.
E-mail address: slong@princeton.edu (S. Long).

0012-821X/$ – see front matter © 2009 Elsevier B.V. All rights reserved.
doi:10.1016/j.epsl.2009.12.033

occur during melt-absent ductile deformation, at temperature conditions necessary for plastic deformation of quartz (300-400 °C (Kerrich et al., 1977; Tullis and Yund, 1977)).

Numerical models based on the Himalayan orogen and Tibetan Plateau make intriguing and testable predictions of large-magnitude, possibly as much as 400–600 km (Beaumont et al. 2001; Jamieson et al., 2006), southward ductile extrusion of the thermally-weakened GH section, which implies coeval and roughly equal displacements across the MCT and STD (Beaumont et al., 2001, 2004; Jamieson et al., 2004, 2006; Beaumont et al., 2006). Bhutan, which lies in the eastern quarter of the Himalayan fold-thrust belt (Fig. 1), is an ideal study site for testing these predictions. Recent studies have interpreted GH sections in eastern Bhutan as a ductile channel that flowed at mid-crustal levels (Davidson et al. 1997; Grujic et al., 2002; Daniel et al. 2003; Hollister and Grujic, 2006). In this study, we present new observations from central Bhutan that reveal significant along-strike changes in the metamorphic and deformational conditions recorded by the GH section.

The goal of this paper is to present new geologic mapping, stratigraphic columns, metamorphic mineral assemblages, U/Pb zircon ages, and structural data which quantify the magnitude, direction and temperature of deformation, that collectively argue for: 1) a depositional contact between the TH and GH sections in central Bhutan, and 2) the presence of a low-grade GH section in central Bhutan that exhibits the kinematic profile of a channel. Our observations contribute to the channel flow debate by 1) placing constraints on the magnitude of displacement on a portion of the STD, and 2) quantifying the magnitude of the top-to-the-north component of channel flow through the upper part of the GH and TH sections. These data test predictions of numerical models for the magnitude of ductile extrusion of the GH section (Beaumont et al. 2001; Jamieson et al. 2006), and have important implications for the role of channel flow as a material transfer mechanism across the Himalayan orogen.

2. Bhutan geologic background

2.1. Greater Himalayan sequence

The GH zone dominates rock exposure in Bhutan (Fig. 1) (Gansser, 1983; Bhargava, 1995). Grujic et al. (2002) divided the Bhutan GH section into a structurally-lower section, between the MCT and the Kakhtang Thrust (KT), and a structurally-higher section, between the KT and the STD (Fig. 1). The structurally-higher level consists of migmatitic orthogneiss, migmatitic metasedimentary rocks, and areally-extensive Miocene leucogranite (Gansser, 1983; Swapp and Hollister, 1991; Davidson et al., 1997; Grujic et al., 2002; Hollister and Grujic, 2006). The structurally-lower GH section is 7–10 km thick, and we divide it into two map units: a lower, 3–9 km-thick granitic orthogneiss unit with schist and paragneiss intervals <200 m thick, and an upper, 1–4 km-thick metasedimentary unit consisting of schist, paragneiss, and quartzite (Figs. 1 and 2). The orthogneiss unit thickens and the metasedimentary unit thins significantly from central to eastern Bhutan (Fig. 1).

Several workers have interpreted both the structurally-lower and higher GH sections in Bhutan as ductile channels that flowed at mid-crustal levels (Davidson et al. 1997; Grujic et al., 2002; Daniel et al., 2003), albeit at different times (Hollister and Grujic, 2006). Observations presented that argue for channel flow include: 1) kinematic evidence for top-to-the-south sense of shear at the base of the section and top-to-the-north sense of shear at the top of the section (Grujic et al., 1996, 2002); 2) synchronous movement on the MCT and STD between 22 and 15.5 Ma (Grujic et al., 2002; Kellett et al., 2009); 3) synchronous movement on the KT and STD between 14 and 11 Ma (Grujic et al., 2002; Kellett et al., 2009); 4) the presence of kyanite and partial melt textures (deformed granitic leucosomes) throughout the section, as well as multiple examples of sillimanite replacing kyanite, indicating peak pressure and temperature conditions of 8–12 kbar and 750–800 °C (Daniel et al., 2003); 5) during deformation, GH rocks were in the sillimanite stability field, and melt was present (Grujic et al., 2002); and 6) metamorphic reactions suggest isothermal (at 600–750 °C) decompression from peak pressures to 5 kbar (Davidson et al., 1997). The significant decrease in rock strength that accompanies partial melting (e.g. Rosenberg and Handy, 2005) is listed as a fundamental prerequisite for channel flow (Grujic, 2006; Hollister and Grujic, 2006; Harris, 2007). Previous data from Bhutan have been limited to the structurally-lower GH section (Grujic et al., 2002; Daniel et al., 2003), near the towns of Lhuentse, Trashigang, and Ura (Fig. 1), or in the structurally-higher GH section above the KT (Swapp and Hollister, 1991; Davidson et al. 1997).

2.2. Tethyan Himalayan sequence and Tethyan-Greater Himalayan contact

The Himalayan tectonostratigraphic zones were originally defined with respect to significant changes in metamorphic grade (Heim and Gansser, 1939; Gansser, 1964). Abrupt juxtaposition of higher-grade rocks over lower-grade rocks was used to define orogen-scale structures such as the MCT and Main Boundary Thrust (MBT) (Heim and Gansser, 1939; Gansser, 1964; LeFort, 1975). Initially, the GH and TH zones were interpreted as a basement-cover sequence, and the contact between them was described as conformable and metamorphically-gradational (Heim and Gansser, 1939; Gansser, 1964, 1983). More recently, workers have identified evidence for a top-to-the-north sense shear zone and/or one or multiple top-to-the-north sense brittle detachment faults that juxtapose the unmetamorphosed to low-grade TH section over the high-grade GH section, which have been termed the STD system (Burg, 1983; Burg et al., 1984; Burchfiel et al., 1992; Searle, 1999; Grujic et al., 2002).

In his pioneering work in Bhutan, Gansser (1964, 1983) recognized several isolated exposures of TH rocks lying above GH rocks, which contain Precambrian (inferred) through Paleozoic sedimentary rocks, and are preserved in the cores of synclines (Fig. 1). Similar large synformal outcrops of TH strata also occur in the central and western Himalaya, and are preserved above klippen of GH rocks (Wadia, 1934; Stocklin and Bhattarai, 1980; Burchfiel et al., 1992; Upreti, 1999; DeCelles et al., 2001; Gehrels et al., 2003; DiPietro and Pogue, 2004; Yin, 2006; Robinson et al., 2006). The basal TH sections in Bhutan contain predominantly non-fossiliferous marble, calcsilicate and schist in the northwest but are more quartzite-rich in central and eastern Bhutan and are referred to as the Chekha Formation (Bhargava, 1995). The Chekha Formation has an inferred Precambrian age due to its lack of fossils and its position at the base of the section (Gansser, 1983; Tangri and Pande, 1995; Bhargava, 1995). The two westernmost isolated TH exposures contain strata as young as Paleozoic (Tang Chu) and Mesozoic (Lingshi syncline) (Gansser, 1983) (Fig. 1).

Gansser (1983) described the contact between the GH and the Chekha Formation as “gradual and conformable”, and he documented that both the uppermost part of GH metasedimentary rocks and the lowermost part of the Chekha Formation contain distinct schist with biotite porphyroblasts (cross-biotites) that are perpendicular to foliation but parallel to lineation. Edwards et al. (1996) suggested that the structurally-high basins recognized by Gansser, particularly the ones that contain Paleozoic strata, may be erosional remnants above the STD. Grujic et al. (2002), based on field observations that supported top-to-the-north sense shear zones at the base of the Chekha Formation, interpreted the Lingshi Syncline, and the Tang Chu, Ura, and Sakteng exposures as klippen soled by the STD (Fig. 1). Grujic et al. (2002) presented the following relationships attributed to all TH–GH contacts in Bhutan: 1) the top of the GH section beneath the STD consists of migmatitic garnet–sillimanite gneiss and schist; 2) top-to-the-north shear sense indicators, including C′-type shear

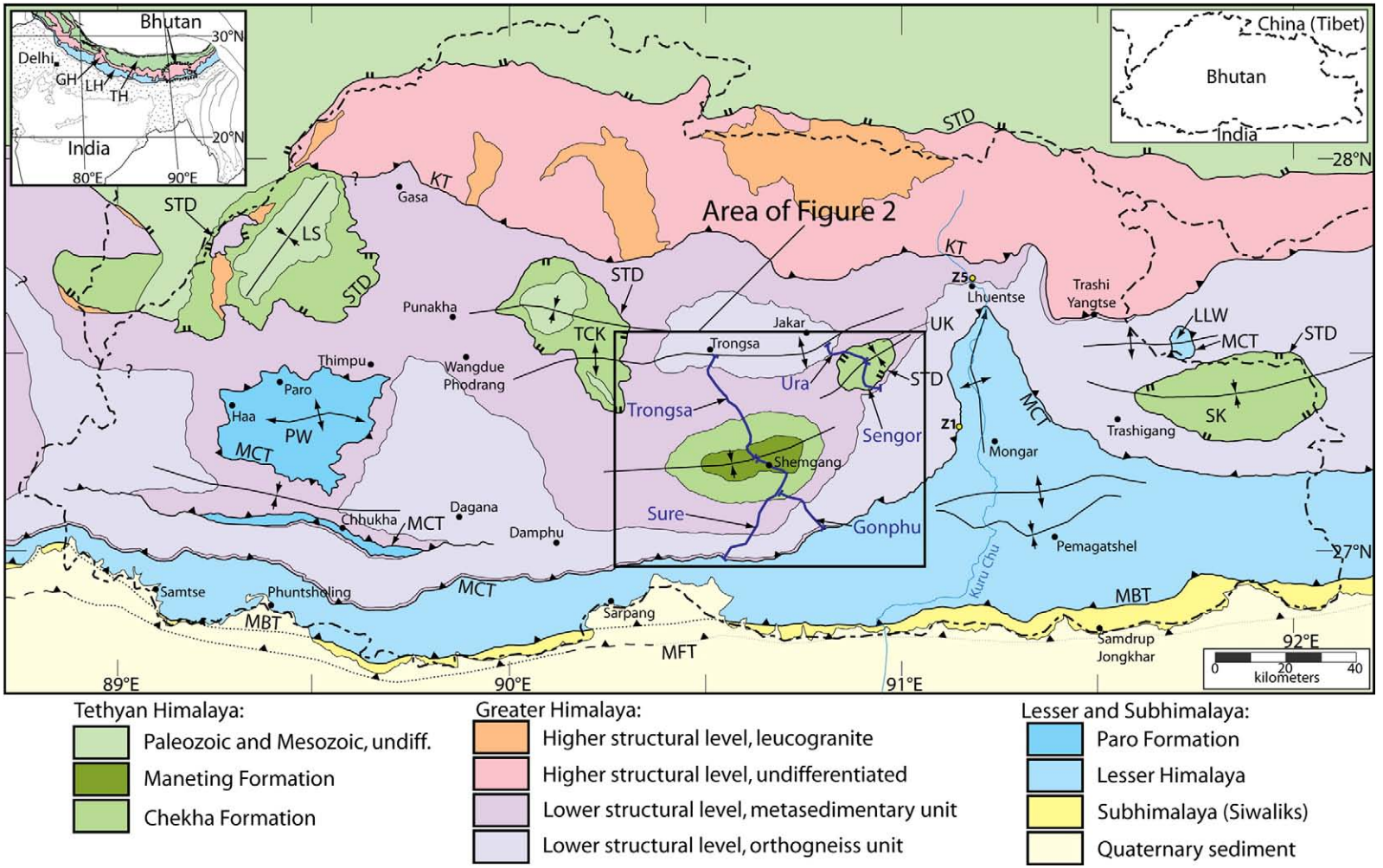

Fig. 1. Simplified geologic map of Bhutan and surrounding region, after Gansser (1983), Bhargava (1995), Grujic et al. (2002), and our own mapping. U-Pb zircon samples located outside of Fig. 2 shown; transect locations and names shown in dark blue. Abbreviations: 1) inset: GH: Greater Himalaya, LH: Lesser Himalaya, TH: Tethyan Himalaya: 2) structures from north to south: STD: South Tibetan Detachment, KT: Kakhtang Thrust, MCT: Main Central Thrust, MBT: Main Boundary Thrust, MFT: Main Frontal Thrust; 3) windows and klippen from west to east: LS: Lingshi Syncline, PW: Paro Window, TCK: Tang Chu Klippe, UK: Ura Klippe, SK: Sakteng Klippe, LLW: Lum La Window (from Yin et al., in press).

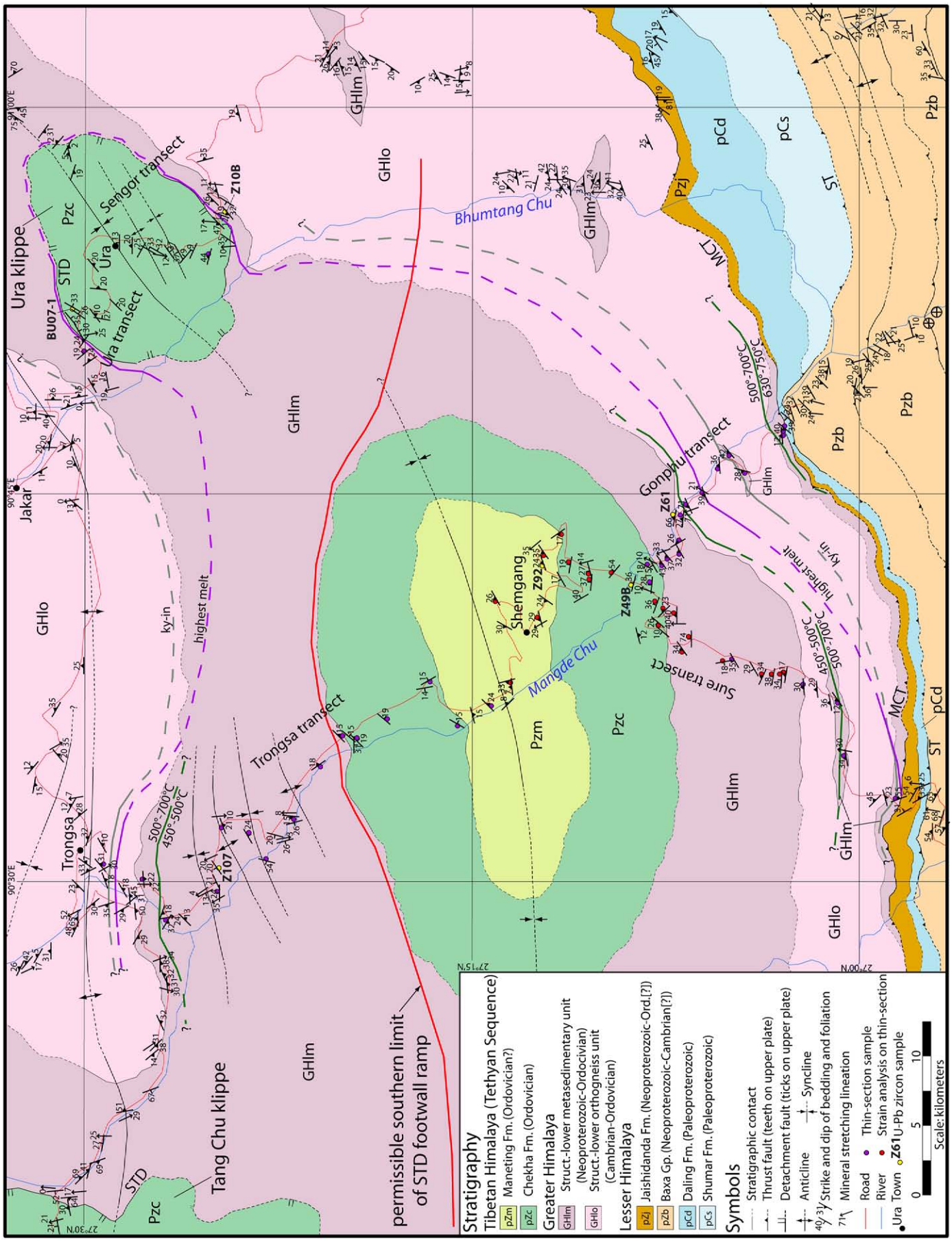
Ura klippe
Sengor transect
Ura transect
Bhumtang Chu
Jakar
Trongsa
Trongsa transect
Tang Chu klippe
STD
MCT
Gomphu transect
Shemgang
Mangde Chu
Sure transect
highest melt
ky-in
500°-700°C
450°-500°C
630°-750°C
permissible southern limit of STD footwall ramp
Stratigraphy
Tibetan Himalaya (Tethyan Sequence)
Maneting Fm. (Ordovician?)
Chekha Fm. (Ordovician)
Greater Himalaya
Struct.-lower metasedimentary unit (Neoproterozoic-Ordocivian)
Struct.-lower orthogneiss unit (Cambrian-Ordovician)
Lesser Himalaya
Jaishidanda Fm. (Neoproterozoic-Ord.[?])
Baxa Gp. (Neoproterozoic-Cambrian[?])
Daling Fm. (Paleoproterozoic)
Shumar Fm. (Paleoproterozoic)
Symbols
Stratigraphic contact
Thrust fault (teeth on upper plate)
Detachment fault (ticks on upper plate)
Anticline
Syncline
Strike and dip of bedding and foliation
Mineral stretching lineation
Road
River
Town
Thin-section sample
Strain analysis on thin-section
U-Pb zircon sample
Scale: kilometers

bands, asymmetric folds, and boudinaged leucogranite dikes, were observed up to 4000 m structural distance below the STD, and overprint the dominant foliation that contains older, synmetamorphic top-to-the south indicators; 3) granitic leucosomes in the centers of shear bands, boudin necks, and flanking folds indicates that melt was present during deformation of GH rocks; 4) non-altered sillimanite in shear bands and on fault surfaces indicates that GH rocks were in the sillimanite stability field during top-to-the-north shearing; 5) at the base of the Chekha Formation, quartzite and garnet–staurolite mica schist have a pervasive tectonic foliation, and asymmetric folds and sheared and rotated leucogranite dikes show a top-to-the-north shear sense; 6) higher in the Chekha Formation section, metamorphic grade decreases, sedimentary bedding becomes the dominant fabric, boudin necks contain quartz rather than melt, and leucogranite dikes are brittlely-deformed, which indicates that top-to-the-north deformation occurred at greenschist facies conditions.

3. Support for a top-to-the-north shear contact at Ura

Our observations in two transects across the Ura klippe, the Ura transect to the north of the syncline axis, and Sengor transect to the south of the syncline axis (Figs. 1 and 2), support the interpretation of a top-to-the-north sense shear zone at the base of the Chekha Formation, in agreement with Grujic et al. (2002). The contact between GH metasedimentary rocks and the Chekha Formation on the Ura transect is marked by an upsection change from paragneiss, quartzite, and schist rich in granitic leucosomes to clean, thick-bedded, cliff-forming Chekha quartzite with muscovite–biotite–garnet schist interbeds, which lack leucosomes (Fig. 3). Here, the contact is marked by a significant change in bedding orientation from northeast-dipping strata below to southeast-dipping strata above (Fig. 4A). Quartzite immediately above the contact displays well-developed, north-trending mineral stretching lineation and axis-preferred, dynamically-recrystallized quartz texture (Fig. 4E). Outcrop-scale top-to-the-north shear sense indicators are observed in GH metasedimentary rocks, and include leucogranite dikes deformed into σ-shapes (Fig. 4B), asymmetric folds (Fig. 4C), and shear cleavage, which we define as a C-type shear band cleavage (Passchier and Trouw, 1998) with secondary foliations (S surfaces) gently inclined relative to bedding planes or primary foliation (C surfaces). Outcrop-scale top-to-the-north shear sense indicators are also observed in the Chekha Formation, and include east-trending, quartz-filled tension gashes in quartzite, oriented perpendicular to mineral stretching lineation when viewed on bedding planes (Fig. 4D), and asymmetric folds in schist (e.g. Stop 210, Fig. 3). Top-to-the-north sense asymmetric folds were observed as high as 1800 m structural distance above the basal contact (e.g. Stop 221, Fig. 3). Biotite–muscovite–garnet mineral assemblages are observed through the full exposed thickness of the Chekha section (Figs. 3 and 4F). On the Sengor transect, southeast of the syncline axis, the contact between Chekha quartzite and GH metasedimentary rocks displays a flat-on-flat relationship of consistently northwest-dipping rocks above and below. A 600 m-thick section of GH metasedimentary rock containing leucosomes and leucogranite dikes is exposed below the contact, which overlies orthogneiss (Fig. 3).

4. Support for a depositional contact at Shemgang

We mapped two transects (Sure and Gonphu) in central Bhutan from the MCT to the axis of an upright syncline that is cored with TH strata, and a third transect (Trongsa) to the north of the syncline axis (Figs. 1–3). The TH strata in this region were mapped in stratigraphic contact with underlying GH rocks by Gansser (1983) and Bhargava (1995), but were mapped in queried fault contact (STD) by Grujic et al. (2002).

The following observations from the Shemgang area, summarized in detail in Sections 4.1, 4.2, and 4.3, support a depositional contact between TH and GH rocks: 1) interfingering of distinct lithologies from the GH metasedimentary unit and the Chekha Formation at their contact, without evidence for brittle faulting or localized shear zones; 2) no abrupt change in metamorphic mineral assemblage through the GH–TH section; 3) broad, low-magnitude shear strain distributed through the GH metasedimentary unit and TH section, a ~14 km total thickness, with no observed zones of high-magnitude or focused shear; and 4) quartz deformation microstructures which suggest gradually decreasing temperatures at 2–4 km above the MCT and similar, but lower temperatures (~450–500 °C) through the rest of the GH and the TH sections, a ~10–12 km total thickness.

4.1. Stratigraphic evidence

On all three transects, the contact between GH and TH map units is conformable, with the orientation of primary foliation in schist, paragneiss, and phyllite subparallel to quartzite bedding (Fig. 2, Suppl. Fig. 4). Sedimentary structures, including cross-bedding (Fig. 5A), imbricated pebbles (Fig. 5C), and compositional lamination, indicate that GH and Chekha quartzite retains original sedimentary bedding and that the section is upright. In addition, low-strain magnitudes in quartzite (Section 4.3.4) argue that bedding has not been transposed. Meso-scale folding (e.g. Fig. 5E) is rare, and gentle to open, map-scale folds are restricted to areas of the Trongsa transect and the syncline axis at Shemgang (Fig. 2). We define the base of the Chekha Formation at the first upsection appearance of continuous, tan, clean, thick-bedded, cliff-forming quartzite.

On the Sure transect, the GH section consists of 3200 m of orthogneiss overlain by 4800 m of metasedimentary rock (Fig. 3). Orthogneiss displays abundant feldspar augen, and contains metasedimentary intervals, including garnet–kyanite schist just above the MCT (Stop 504, Fig. 3). This schist is intruded by an undeformed, non-foliated leucogranite sill. The base of the GH metasedimentary unit consists of 800 m of biotite–garnet paragneiss overlain by 500 m of micaceous quartzite. Trough cross-bedding preserved in quartzite shows that the beds are upright (e.g. Fig. 5A). We also observe interfingering of GH schist and quartzite (Fig. 5B). Muscovite–biotite schist throughout the GH metasedimentary unit contains distinct foliation-perpendicular biotite porphyroblasts ('cross-biotites' on Figs. 3 and 7D, E), and often contains garnet. The distinctive biotite porphyroblast schist alternates with the clean, white, cliff-forming quartzite of the Chekha Formation over a structural distance of 1100 m, with the quartzite becoming more common upsection (Stops 485, 521, and 522, Fig. 3). We observe no evidence for brittle faulting or concentrated shear at the contacts between alternating quartzite and schist lithologies, which would be predicted in the case of structural interleaving at a brittle detachment. Shear cleavage does develop in schist interbeds between quartzite layers (e.g. Fig. 5D) and is always top to the south (see details in Section 4.3.1). The Chekha Formation is 3700 m thick on the Sure transect, and consists of tan to white, thick-bedded, fine- to medium-grained, cliff-forming, locally conglomeratic (Fig. 5C) quartzite. Quartzite is clean, generally containing less than 5–10% muscovite and biotite, and garnet is rare. Upright bedding is indicated by common cross-bedding (e.g. Fig. 5A); these upright indicators combined with only open-gentle

Fig. 2. Geologic map of part of central and east-central Bhutan; location shown on Fig. 1. See Fig. 1 caption for structure abbreviations (ST is Shumar Thrust). Boundaries between quartz recrystallization regimes, and associated temperature constraints (see Section 4.3.3) are indicated by colored solid (observed) and dashed (inferred) lines; also shown are upper limit of partial melt textures (lower limit is MCT), and kyanite-in isograd. Thick red solid line represents southern permissible location of STD footwall ramp.

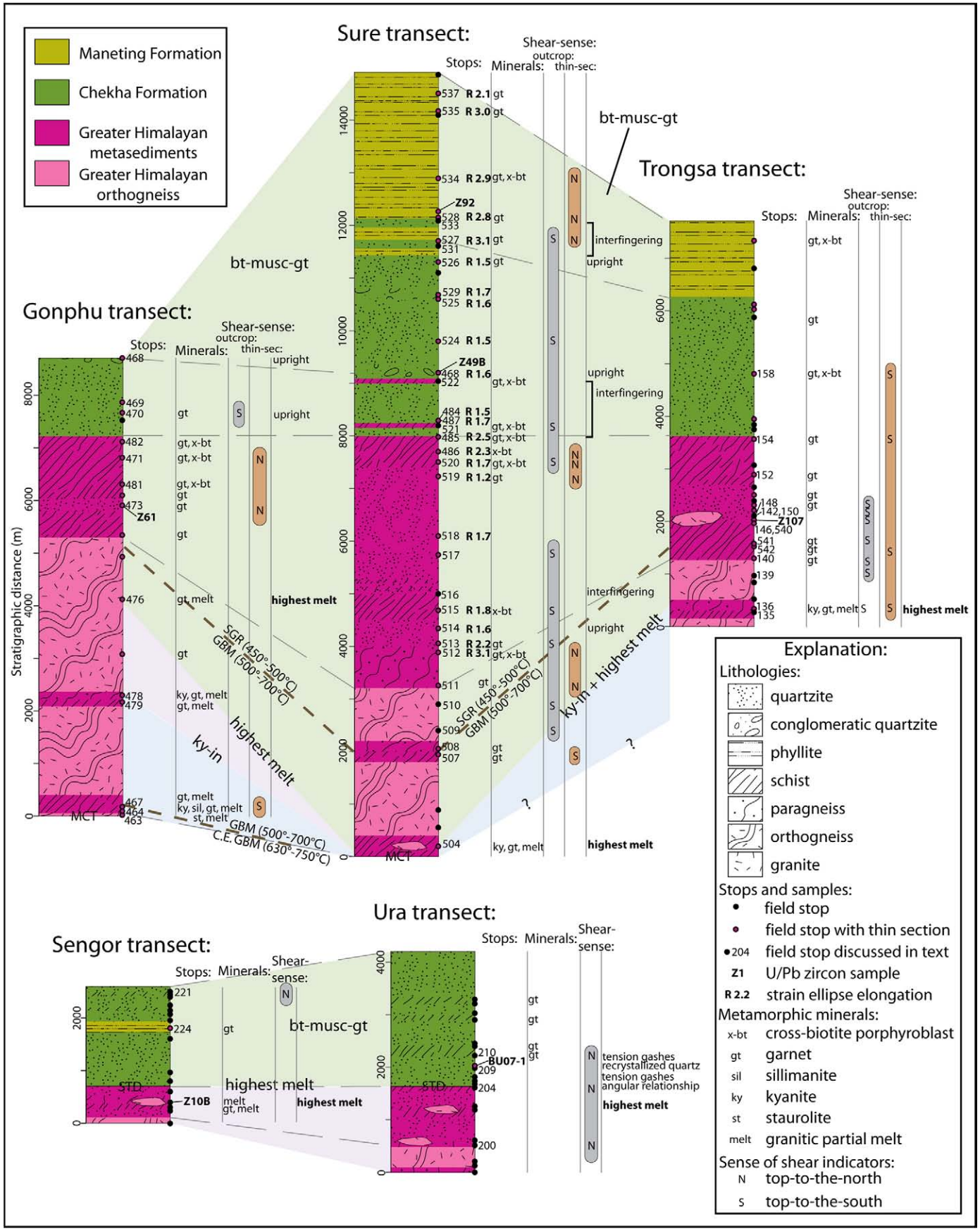
Maneting Formation
Chekha Formation
Greater Himalayan metasediments
Greater Himalayan orthogneiss
Sure transect:
Trongsa transect:
Gonphu transect:
Sengor transect:
Ura transect:
Stops:
Minerals:
Shear-sense:
outcrop:
thin-sec:
bt-musc-gt
interfingering
upright
highest melt
ky-in
ky-in + highest melt
SGR (450°-500°C)
GBM (500°-700°C)
GBM (500°-700°C)
C.E. GBM (630°-750°C)
MCT
STD
Stratigraphic distance (m)
Explanation:
Lithologies:
quartzite
conglomeratic quartzite
phyllite
schist
paragneiss
orthogneiss
granite
Stops and samples:
field stop
field stop with thin section
field stop discussed in text
U/Pb zircon sample
strain ellipse elongation
Metamorphic minerals:
cross-biotite porphyroblast
garnet
sillimanite
kyanite
staurolite
granitic partial melt
Sense of shear indicators:
top-to-the-north
top-to-the-south
tension gashes recrystallized quartz
tension gashes angular relationship

(interlimb angles of 90–170°) map-scale folds (Fig. 2) and rare mesoscale folding (e.g. Fig. 5E) indicates that the entire section is upright. The contact between the Chekha and Maneting formations is marked by the upsection transition to dark-gray, graphitic, finely-laminated, biotite–garnet phyllite. We observe these alternating lithologies over a structural distance of 800 m, indicating an interfingering relationship (e.g. Fig. 5B). 3200 m of Maneting Formation phyllite is exposed along the Sure transect, until the syncline axis is reached.

On the Gonphu transect, the GH section consists of 5300 m of orthogneiss overlain by 1900 m of metasedimentary rock. The orthogneiss unit contains abundant feldspar augen and local garnet, and contains two metasedimentary intervals, including staurolite–garnet schist and kyanite–sillimanite–garnet schist between 100 and 400 m above the MCT (Stops 463, 464, and 467, Fig. 3), and kyanite–garnet schist between 2000 and 2300 m above the MCT (Stops 479 and 478, Fig. 3). The GH metasedimentary unit consists of muscovite–biotite–garnet schist interbedded with micaceous quartzite. The top 900 m of GH metasedimentary rock consists of schist with distinct foliation-perpendicular biotite porphyroblasts (Stops 481, 471, and 482, Fig. 3), similar to the lithology observed on the Sure transect. The contact with the Chekha Formation is marked by an abrupt change to tan, thick-bedded, cliff-forming quartzite, without interfingering as observed on the Sure transect. Cross-bedding preserved in Chekha quartzite shows an upright orientation (e.g. Stop 470, Fig. 3).

On the Trongsa transect, a minimum thickness of 1250 m of orthogneiss is overlain by 2350 m of GH metasedimentary rock. The orthogneiss unit contains one metasedimentary interval of melt-bearing, kyanite–garnet schist and biotite-rich paragneiss (Stops 135 and 136, Fig. 3). The GH metasedimentary unit consists of muscovite–biotite–garnet schist interbedded with micaceous quartzite. The transition to the Chekha Formation is marked by a change from muscovite–biotite–garnet GH schist to white-tan, thick-bedded, fine- to medium-grained quartzite. Again, Chekha quartzite generally has less than 10% muscovite and biotite, and garnet is rare. The upper contact with the Maneting Formation is marked by an abrupt change to dark-gray, graphitic, biotite–garnet phyllite, and lacks the interfingering relationship observed on the Sure transect. 1500 m of Maneting Formation phyllite is exposed on the Trongsa transect, before the syncline axis is reached.

We obtained U/Pb zircon data (Suppl. Discussion 1, Suppl. Fig. 1) from both TH and GH rocks to test whether there was a pronounced change in age or provenance of detrital zircon (DZ) grains between strata mapped as Chekha Formation and strata mapped as the GH metasedimentary unit. U/Pb zircon data from GH orthogneiss indicates a Cambro-Ordovician (487 ± 7 Ma, 1σ) crystallization age of the augen gneiss' granitic protolith (sample Z1, Fig. 1; Suppl. Fig. 2A). This interpretation is supported by the presence of Cambrian–Ordovician intrusive bodies in GH rocks throughout the orogen (e.g. Gehrels et al., 2003; Cawood et al., 2007). U/Pb age spectra of DZ also limit the deposition ages of GH sedimentary protoliths. We obtained DZ peaks as young as ~460 Ma (sample Z61) and ~500 Ma (sample Z104) on the lowest quartzite within the GH metasedimentary unit (Figs. 2 and 3). However, the presence of additional metasedimentary intervals within the GH orthogneiss unit indicates that GH sedimentary protoliths had to exist prior to Cambrian–Ordovician intrusion of the orthogneiss' granitic protoliths. The ~900 Ma youngest DZ peak age from quartzite sample Z5 (Fig. 1) may bracket the oldest permissible deposition age of GH sedimentary protoliths in Bhutan as Neoproterozoic. U/Pb DZ age spectra from Chekha Formation quartzite in the Shemgang region (sample Z49B, Figs. 2 and 3) displays a youngest peak centered at ~460 Ma, which indicates an Ordovician maximum deposition age, and is indistinguishable within error from the youngest peak age of GH quartzite.

4.2. Metamorphic evidence

On the Sure transect, kyanite and partial melt textures are only observed in a basal metasedimentary interval in the GH orthogneiss unit, <200 m above the MCT (Stop 504, Fig. 3). Above this level, the entire 15 km-thick Sure transect, including the GH metasedimentary unit and Chekha and Maneting Formations, contains rocks with biotite–muscovite–garnet assemblages (Fig. 6C, E, F).

On the Gonphu transect, a schist interval within the orthogneiss unit 100 m above the MCT contains staurolite (Stop 463, Fig. 3), displays bent and dismembered kyanite (Fig. 6A), and fibrolitic sillimanite growing in garnet pressure shadows (Fig. 6B). In addition, metasedimentary intervals within the GH orthogneiss unit contain multiple plagioclase-rich leucosomes (Stops 467 and 479, Fig. 3). A paragneiss interval 2300 m above the MCT contains the highest occurrence of kyanite (Stop 478, Fig. 3), and orthogneiss 4100 m above the MCT displays the highest observed occurrence of partial melt texture (Stop 476, Fig. 3). Upsection from this level, the entire Gonphu transect contain rocks with garnet–biotite–muscovite assemblages.

On the Trongsa transect, a paragneiss interval within the GH orthogneiss unit, 900 m below the upper contact, displays kyanite and granitic leucosomes (Stop 136, Fig. 3). This is the highest observed occurrence of kyanite and partial melt on the transect. As in the Gonphu and Sure transects, all rocks stratigraphically above this level display biotite–muscovite–garnet mineral assemblages (Fig. 6D).

Temperature and pressure conditions reported for GH sections in eastern Bhutan include 8–10 kbar and 650 °C for staurolite- and melt-bearing intervals at the base of the section (Daniel et al., 2003). Peak metamorphic conditions estimated for kyanite- and melt-bearing GH intervals in eastern Bhutan are as high as 10–12 kbar and 750–800 °C (Daniel et al., 2003). Broad temperature constraints can be placed on the biotite–muscovite–garnet bearing sections that we observe in central Bhutan, and range between ~475 °C, the minimum temperature required to form garnet at pressures >1 kbar (Spear and Cheney, 1989) to ~675 °C, the muscovite dehydration-melting reaction at 4–7 kbar (Spear and Cheney, 1989). Note that the presence of water as a free fluid phase would lower partial melting temperatures by ~25 °C at ~7 kbar (Spear et al., 1999). More precise temperature constraints come from quartz recrystallization microstructure and are described in Section 4.3.3.

4.3. Structural evidence

4.3.1. Outcrop-scale kinematic indicators

At the outcrop-scale, top-to-the-south sense kinematic indicators dominate all three transects. On the Sure transect, these include feldspar augen σ-clasts in the GH orthogneiss unit (Stops 509 and 510, Fig. 3), and shear fractures in quartzite (Stops 513 and 524, Fig. 3), shear cleavage in schist and phyllite (Stops 515, 520, 521, and 531, Fig. 3), and asymmetric folds in schist (Stops 517 and 520, Fig. 3) throughout the GH metasedimentary unit and Chekha Formation. On

Fig. 3. Stratigraphic columns for transects in the Shemgang (Gonphu, Sure, Trongsa) and Ura (Sengor, Ura) areas. Refer to Figs. 1 and 2 for map locations. Dashed tie lines connect similar stratigraphic and structural positions between transects. Columns on right side of each section show: 1) stratigraphic locations of metamorphic mineral assemblages and partial melt textures (note: biotite and muscovite are present at all stratigraphic levels, and only locations of distinct cross-biotite porphyroblasts are listed). 2) All kinematic indicators for Ura and Sengor transects were observed at outcrop scale. 3) Ellipticity ratio (R) of tectonic strain ellipse in X–Z strain plane shown for samples in Sure transect. Blue shaded area represents part of section below kyanite—in line; pink shaded area represents part of section below highest partial melt texture, and green shaded area represents part of section with biotite–muscovite–garnet assemblages. Stratigraphic positions of boundaries between quartz recrystallization mechanisms (and associate temperature constraints) are indicated (see Section 4.3.3 for abbreviations and discussion).

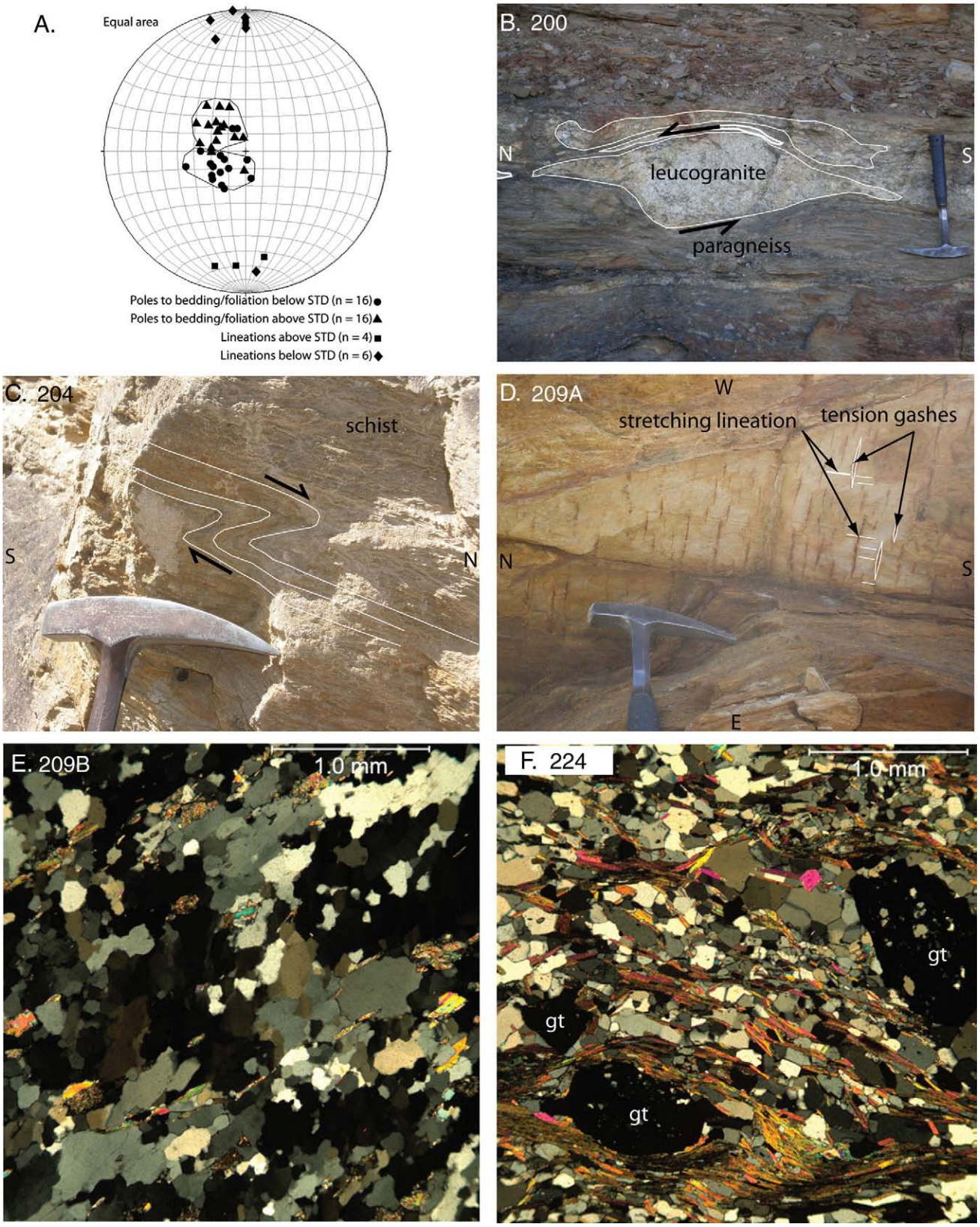

Fig. 4. Pictures and photomicrographs (cross-polarized light) from Ura area. Stop numbers referenced on Fig. 3. All distances listed are structural thicknesses. A) Equal-area stereographic projection showing change in bedding and foliation orientation above and below STD on Ura transect. B) Stop 200: Leucogranite dike in paragneiss interval in GH orthogneiss unit, deformed into top-to-north sense σ-shape, 1500 m below STD on Ura transect; 30 cm hammer for scale. C) Stop 204: Top-to-north sense asymmetric fold in GH schist, 40 m below STD on Ura transect; 15 cm hammer head for scale. D) Stop 209A: Lineation-perpendicular tension gashes viewed on base of Chekha quartzite bedding plane, 300 m above STD on Ura transect; 15 cm hammer head for scale. E) Stop 209B: Photomicrograph showing SGR recrystallization texture of Chekha quartzite, 300 m above STD on Ura transect. F) Stop 224: Photomicrograph of biotite–garnet phyllite on Sengor transect, 1100 m above STD.

Fig. 5. Photographs of sedimentary structures and field relationships (A–C) and outcrop-scale kinematic indicators (D–F) in Shemgang area. Stop numbers referenced on Fig. 3. All distances listed are structural thicknesses; directions labeled on photographs D–F. A) Stop 514: Upright trough cross-bedding in quartzite of GH metasedimentary unit, 1150 m above lower contact on Sure transect. B) Stop 516: Interfingering of quartzite and schist in GH metasedimentary unit; 1800 m above lower contact on Sure transect. C) Stop 468: Imbricated pebbles in conglomeratic Chekha quartzite, 1200 m above basal contact on Sure transect; 15 cm hammer head for scale. D) Stop 470A: Top-to-south sense shear cleavage in schist interbed in Chekha Formation, 450 m above lower contact on Gonphu transect. E) Stop 540: Top-to-south sense asymmetric fold in schist in GH metasedimentary unit, 800 m structural distance above lower contact on Trongsa transect. F) Stop 146: Top-to-south sense duplexing in quartzite of GH metasedimentary unit, 800 m above lower contact on Trongsa transect.

the Gonphu transect, these include shear cleavage in schist (Fig. 5D), and outcrop-scale duplexing of quartzite beds (Stop 470, Fig. 3) in the Chekha Formation. On the Trongsa transect, these include leucosomes deformed into σ-shapes (Stop 136, Fig. 3) and feldspar augen σ-clasts (Stop 139, Fig. 3) in the GH orthogneiss unit, and shear cleavage (Stops 148, 150, and 541, Fig. 3) and asymmetric folds (Fig. 5E, Stops 140 and 540, Fig. 3) in schist, and outcrop-scale duplexing of quartzite beds (Fig. 5F) in the GH metasedimentary unit. Penetrative mineral stretching lineation is ubiquitous in the GH orthogneiss unit, and is common in schist and paragneiss lithologies in the lower portions of the

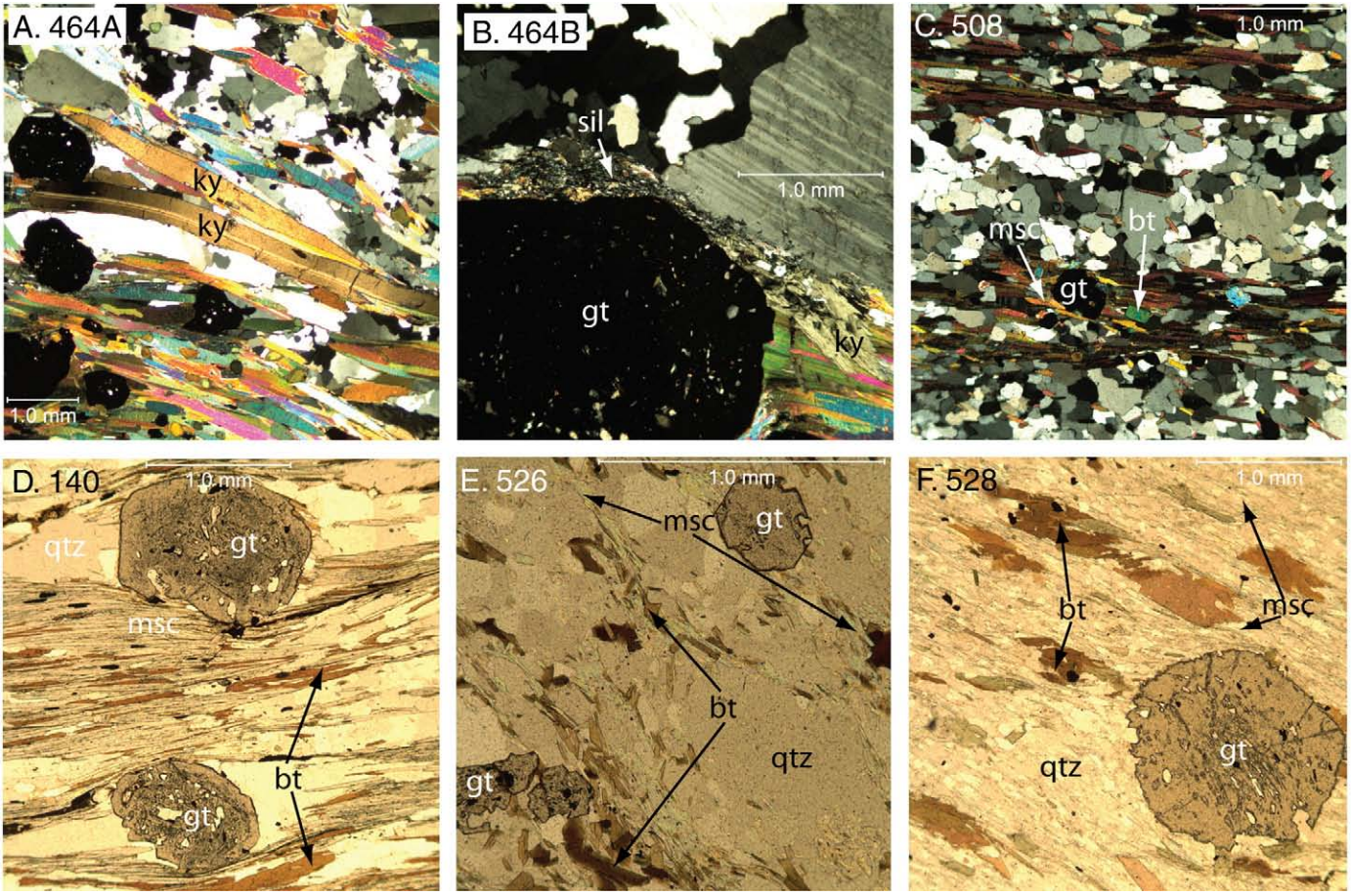

Fig. 6. Photomicrographs of metamorphic mineral assemblages from Shemgang area, shown in stratigraphic order from lowest to highest; A–C in cross-polarized light, D–F in plane polarized light. All thin sections cut perpendicular to bedding or primary foliation, and parallel to mineral stretching lineation. Stop numbers referenced on Fig. 3. All distances listed are structural thicknesses. A) Stop 464A: Bent and deformed kyanite blades in schist interval within GH orthogneiss unit, 100 m above MCT on Gonphu transect. B) Stop 464B: Fibrolite sillimanite growing in garnet pressure shadow. Note kyanite present; 100 m above MCT on Gonphu transect. C) Stop 508: Paragneiss interval in GH orthogneiss unit displaying quartz, garnet, muscovite, and biotite; 2050 m above MCT on Sure transect. D) Stop 140: Schist from GH metasedimentary unit displaying quartz, garnet, muscovite, and biotite; 70 m above lower contact on Trongsa transect. E) Stop 526: Chekha Formation quartzite displaying quartz, garnet, muscovite, and biotite; 3300 m above lower contact on Sure transect. F) Stop 528: Maneting Formation phyllite displaying quartz, garnet, muscovite, and biotite; 450 m above lower contact on Sure transect.

GH metasedimentary unit. However, lineation is rare in GH quartzite, and is generally absent in Chekha Formation quartzite.

These outcrop-scale structures (Fig. 5D–F) are distributed throughout the three transects and are never concentrated in a discrete zone like that observed for the STD at Ura. In addition, all indicate top to south transport. It is important to emphasize that we do not observe zones of highly-sheared rock at the outcrop scale, nor do we observe more localized highly-strained zones, particularly across the thick section of alternating schist and quartzite lithologies at the GH-Chekha contact or at the top of the GH orthogneiss unit (in addition see Section 4.3.4).

We interpret these outcrop-scale kinematic indicators, which include a combination of ductile (asymmetric folds and shear cleavage in schist) and brittle deformation features (shear fractures and duplexing in quartzite) as cooler structural overprints that we attribute to top-to-the-south deformation that most likely post-dates more diffuse, ductile, thin-section-scale fabrics discussed in the following sections.

4.3.2. Thin-section scale kinematic indicators

Kinematic indicators observed at the thin-section scale on the Sure and Gonphu transects divide the GH and TH section into a lower domain displaying a top-to-the-south shear sense and an upper domain displaying a top-to-the-north shear sense (summarized on Fig. 3). Top-to-the-south sense kinematic indicators include a C′-type shear band (Fig. 7A) and muscovite fish (Fig. 7B) in the GH orthogneiss unit, and top-to-the-north sense indictors include rotated garnet porphyroblasts (Stops 511, 485, and 528, Figs. 3 and 7C), rotated biotite porphyroblasts (Stop 520, Figs. 3 and 7D, E, F), asymmetric folds (Fig. 7G), CS fabric (Fig. 7H), and offset of older foliation by younger crenulation cleavage (Stop 527, Fig. 3) in the GH metasedimentary unit and Maneting Formation.

Taken together, thin-section scale kinematic indicators define a 2–3 km-thick section of top-to-the-south shear overlain by a ~11 km-thick section of top-to-the-north shear (Fig. 3). We interpret this to represent the profile of an asymmetric "channel," with the greatest displacement in the direction of transport at the change in shear sense (Fig. 9B). The asymmetry in thickness of the kinematic domains skews the greatest displacement towards the base of the section, which requires a variable viscosity through the channel, with the lowest viscosity at the base. A low-viscosity base is supported observationally by the presence of partial melt textures just above the MCT. We interpret these thin-section scale kinematic indicators, which are universally ductile features (shear bands, mica fish, CS fabric, asymmetric folds, rotated porphyroblasts, etc.) as syn-deformational features that likely occurred at the same time as the formation of ca. 450–700 °C quartz deformation textures that we document in Sections 4.3.3 and 4.3.4.

In contrast to the Sure and Gonphu transects, the GH and TH sections on the Trongsa transect display only top-to-the-south sense kinematic indicators, including muscovite fish (Stop 136, Fig. 3), rotated garnet porphyroblasts (Stops 542 and 158, Fig. 3), and asymmetric folds (Stop 154, Fig. 3).

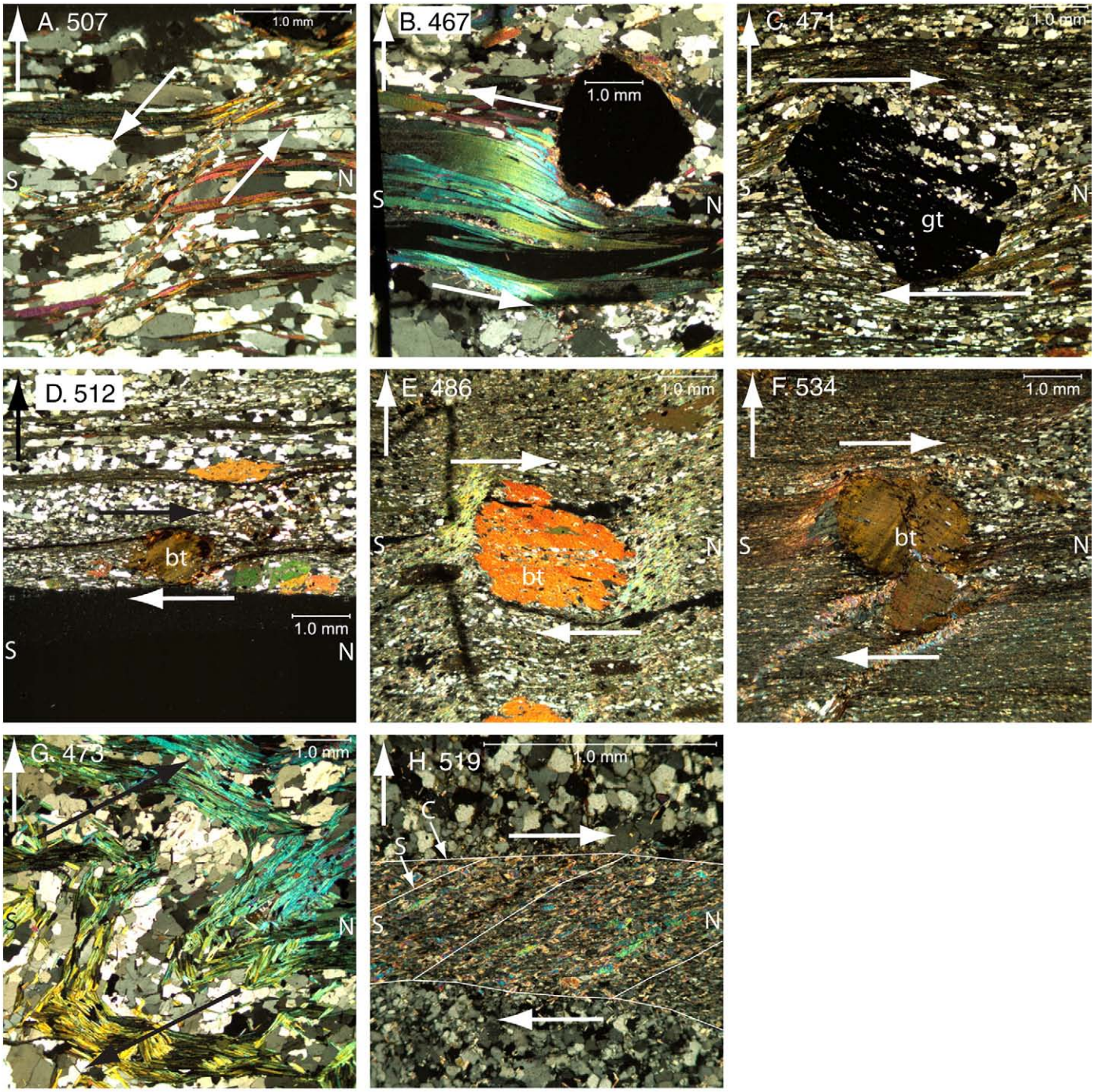

Fig. 7. Photomicrographs of thin-section scale kinematic indicators from Shemgang area (cross-polarized light). All thin sections cut perpendicular to bedding or primary foliation, and parallel to mineral stretching lineation. Stop numbers referenced on Fig. 3. All distances listed are structural thicknesses. Arrow in upper left corner points to stratigraphic up, and N and S directions are labeled. A) Stop 507: Top-down-to-south sense C′-type shear band in schist in metasedimentary interval within GH orthogneiss unit, 1950 m above MCT on Sure transect. B) Stop 467: Top-to-south sense muscovite fish in schist interval within GH orthogneiss unit, 200 m above MCT on Gonphu transect. C) Stop 471: Top-to-north sense rotated garnet in schist in GH metasedimentary unit, 1530 m above lower contact on Gonphu transect. D) Stop 512: Top-to-north sense rotated biotite porphyroblast in paragneiss in GH metasedimentary unit, 700 m above basal contact on Sure transect. E) Stop 486: Top-to-north sense rotated biotite porphyroblast in schist in GH metasedimentary unit, 4500 m above basal contact on Sure transect. F) Stop 534: Top-to-north sense rotated biotite porphyroblast in Maneting phyllite, 1200 m above basal contact on Sure transect. G) Stop 473: Top-to-north sense asymmetric folds in alternating muscovite and quartz microlithons in paragneiss in GH metasedimentary units, 630 m above lower contact on Gonphu transect. H) Stop 519: Top-to-north sense CS fabric in quartzite in GH metasedimentary unit, 4050 m above basal contact on Sure transect.

4.3.3. Quartz microstructure

Quartz recrystallization microstructure in GH and TH rocks at Shemgang records a decrease in deformation temperatures from the MCT up through the section. Rocks just above the MCT display evidence for quartz recrystallization through grain boundary migration (GBM), which occurs between ~500 and 700 °C (Stipp et al., 2002), and transition upsection to subgrain rotation (SGR) quartz recrystallization, which occurs between ~400 and 500 °C (Stipp et al., 2002). The transition to SGR recrystallization occurs in a different stratigraphic level on each transect (Figs. 2 and 3).

On the Gonphu transect, the entire GH orthogneiss unit shows evidence for GBM recrystallization (Figs. 2 and 3). Characteristic GBM texture consists of amoeboid grains with highly-irregular, interfingering boundaries, often with large (multiple mm) recrystallized grain

size (Fig. 8B). Melt-bearing, kyanite–sillimanite–garnet schist ~100 m above the MCT displays 'chessboard extinction' (Kruhl, 1996; Stipp et al., 2002), with square subgrains with boundaries roughly parallel to grain boundaries (Fig. 8A). Chessboard extinction has been interpreted to represent basal <a> and prism [c] slip (Mainprice et al., 1986; Blumenfeld et al., 1986), and is estimated to occur at temperatures ranging between

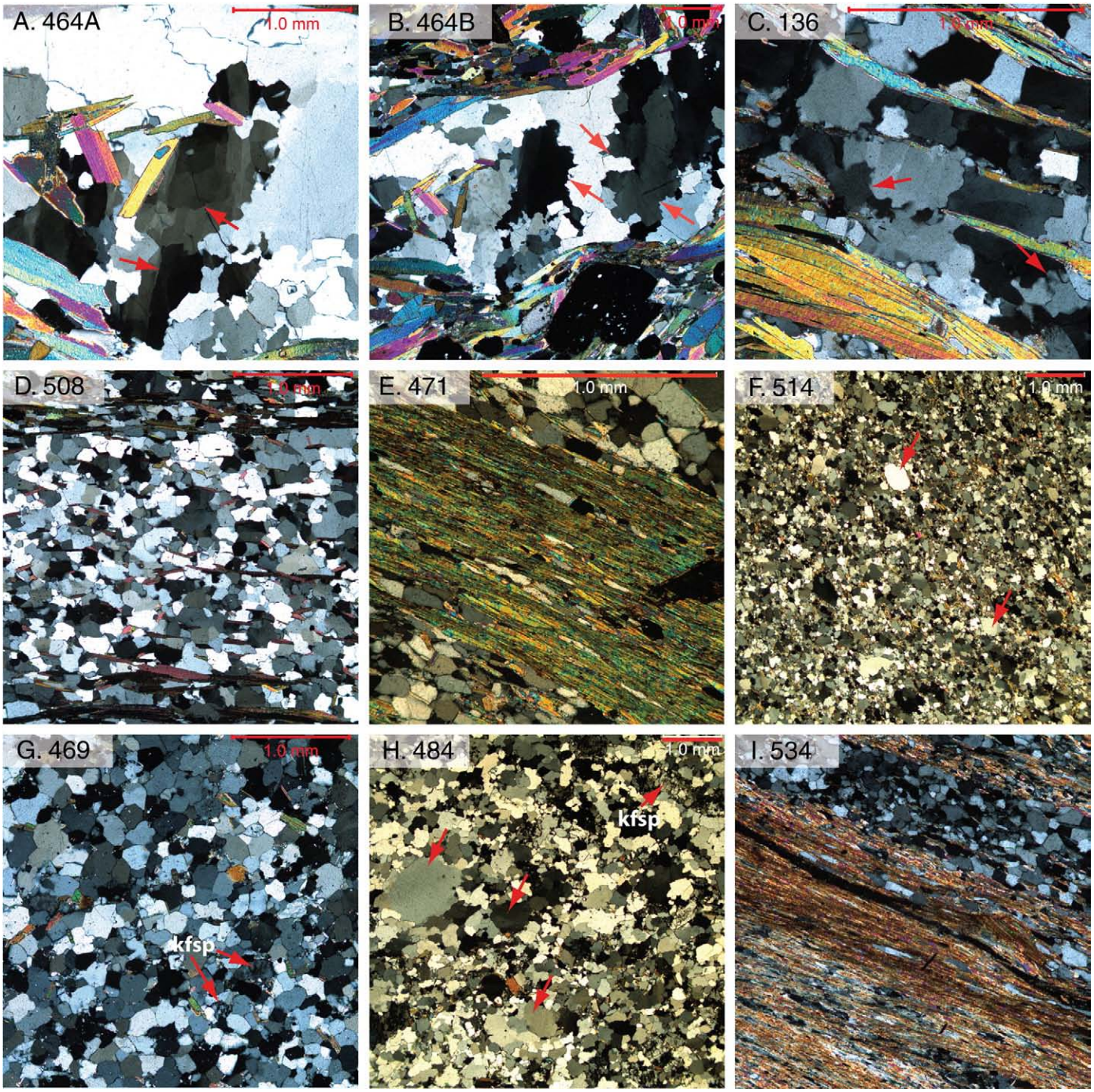

Fig. 8. Photomicrographs illustrating deformation microstructure in GH and TH rocks near Shemgang; cross-polarized light. All thin sections cut perpendicular to bedding or primary foliation, and parallel to mineral stretching lineation. Shown in stratigraphic order from lowest to highest; all stop numbers shown on Fig. 3. A) Stop 464A: Grain boundary migration (GBM) chessboard extinction (square subgrains) in schist in GH orthogneiss unit, 100 m above MCT on Gonphu transect; indicates minimum deformation temperatures of ca. 630–650 °C. B) Stop 464B: Amoeboid-grain quartz microstructure characteristic of GBM recrystallization; in GH orthogneiss unit, 100 m above MCT on Gonphu transect. Note large (1–4 mm) recrystallized grain size. C) Stop 136: Amoeboid-grain GBM microstructure in GH orthogneiss unit; 900 m below upper contact on Trongsa transect. D) Stop 508: Equigranular, polygonal 'foam' subgrain rotation (SGR) microstructure; from metasedimentary interval in GH orthogneiss unit, 2050 m above MCT on Sure transect. E) Stop 471: Quartz microstructure characteristic of schist and paragneiss of GH metasedimentary unit; note equigranular, polygonal SGR microstructure of quartz-dominated microlithons, and lack of recrystallization of quartz grains isolated in mica-dominated microlithon. Also note difference in aspect ratios between isolated quartz grains and recrystallized quartz grains; 400 m below upper contact on Gonphu transect. F) Stop 514: Quartzite from GH metasedimentary unit displaying partial SGR recrystallization. Relic porphyroclasts marked with arrow; 1150 m above lower contact on Sure transect. G) Stop 469: Chekha Formation quartzite exhibiting low-strain, non-recrystallized quartz microstructure; quartz grain-to-grain contacts interpreted as original. Note lack of K-feldspar deformation, and random orientation of biotite porphyroblasts; 650 m above lower contact on Gonphu transect. H) Stop 484: Chekha Formation quartzite exhibiting ~80% SGR quartz recrystallization into polygonal subgrains; relic porphyroclasts marked with arrows. Note recrystallized K-feldpsar; 300 m above lower contact on Sure transect. I) Maneting Formation phyllite displaying equigranular, polygonal SGR quartz microstructure in quartz-dominated microlithons, and non-recrystallized, plastically-elongated, isolated quartz grains in mica-dominated microlithons. Note difference in aspect ratio between isolated quartz grains and recrystallized quartz microlithons; 1200 m above lower contact on Sure transect.

~630 °C minimum (Stipp et al., 2002) and 650–750 °C (Lister and Dornsiepen, 1982; Mainprice et al., 1986).

The upsection transition from GBM to SGR-dominated recrystallization occurs near the top of the orthogneiss unit on the Gonphu transect (Figs. 2 and 3). On the Sure transect, this transition occurs at a lower level, within the GH orthogneiss unit (Figs. 2 and 3). Here, amoeboid-grain GBM textures are observed as high as 1950 m above the MCT (Stop 507, Fig. 3). However, 2050 m above the MCT (Stop 508, Fig. 3), muscovite–biotite–garnet schist exhibits a granoblastic 'foam' microstructure (Schmid, 1994), with equigranular, polygonal quartz grains (Fig. 8D) indicative of SGR recrystallization. On the Trongsa transect, amoeboid-grain GBM textures are observed in the upper part of the orthogneiss unit (Fig. 8C) and base of the metasedimentary unit, and the upsection transition to SGR recrystallization occurs ca. 300 m above the lower GH metasedimentary unit contact (Figs. 2 and 3).

Everywhere above the GBM-SGR transition, GH and TH sections display SGR-dominated quartz microstructure through their full exposed thickness. Quartz-dominated microlithons in GH schist and paragneiss and Maneting Formation phyllite characteristically display equigranular, polygonal quartz microstructure indicative of SGR recrystallization (Fig. 8E, I). However, in these lithologies, quartz grains isolated within muscovite- and biotite-dominated microlithons are typically non-recrystallized and plastically-elongated, with a shape-preferred orientation subparallel to primary foliation (Fig. 8E, I). Aspect ratios of isolated quartz grains are consistently longer that those of recrystallized subgrains in quartz-dominated microlithons. Quartzite of the GH metasedimentary unit displays equigranular, polygonal quartz microstructure typical of SGR recrystallization, with a shape-preferred orientation at a low angle (<30°) to bedding (Fig. 8F). However, the majority of GH quartzite samples are not completely recrystallized, and still exhibit relic quartz grains (porphyroclasts) (Fig. 8F). Quartz microstructure in Chekha Formation quartzite varies between partial SGR recrystallization (Fig. 8H) and low-strain, non-recrystallized textures (Fig. 8G). The majority of Chekha samples exhibit ca. 60–90% quartz recrystallization into equigranular, polygonal subgrains, but larger porphyroclasts are preserved, which results in a range of grain size (Fig. 8H). Both subgrains and porphyroclasts in Chekha quartzite typically display a shape-preferred orientation situated subparallel or at <30° to bedding.

Recrystallization of K-feldspar into multiple subgrains (Fig. 8H) is observed through the full thickness of the Chekha Formation. K-feldspar recrystallization indicates minimum deformation temperatures of ~450 °C (White, 1975; Voll, 1976; Simpson and Wintsch, 1989), and SGR quartz recrystallization represents maximum deformation temperatures of ~500 °C (Stipp et al., 2002).

In eastern Bhutan, deformation temperatures of 650–750 °C from quartz CPO plots of GH samples (Lister and Dornsiepen, 1982; Mainprice et al., 1986; Grujic et al., 1996) indicate that deformation occurred at peak metamorphic temperatures, which were estimated between 650 and 800 °C from equilibrium mineral assemblages (Daniel et al., 2003). Our data from the Shemgang region show that the majority of the GH section and full TH section experienced deformation at peak temperatures of 450–500 °C, which is in good agreement with the ~475 °C minimum temperature required to form garnet (Spear and Cheney, 1989). Together these data require along-strike changes of ~250–300 °C between the cooler GH–TH section in central Bhutan and the hotter GH section in eastern Bhutan. Only kyanite- and melt-bearing rocks within 100 m of the MCT on the Gonphu transect experienced similar peak temperature conditions (ca. 630–750 °C) to those reported for GH rocks in eastern Bhutan (Daniel et al., 2003).

4.3.4. Finite strain data in Sure transect

To estimate the strain magnitude through the ~11 km-thick GH and TH section on the Sure transect that displays a top-to-the-north shear sense, we performed fabric analyses of quartz grains. We analyzed 21 thin sections that were cut perpendicular to bedding or primary foliation and parallel to mineral stretching lineation, representing the *X–Z* strain plane. Thin sections from the same samples, cut perpendicular to bedding or foliation and perpendicular to stretching lineation, representing the *Y–Z* strain plane, were also analyzed, and indicate deformation in a moderate flattening to plane 3D strain field. In GH schist and Maneting Formation phyllite, the Rf-phi method (Ramsay and Huber, 1983) was used on elongated, non-recrystallized quartz grains isolated within mica-dominated microlithons (Fig. 8E, I), with approximately 30 grains measured per thin section. While strength differences between mica- and quartz-dominated microlithons can result in heterogeneous deformation for these lithologies, we argue that these techniques provide a valid estimate for bulk strain in these rocks. The Rf-phi method was also used on relic porphyroclasts (Fig. 8F, H) in partially-recrystallized GH and Chekha quartzite, with 20–30 grains measured per thin section. Finally, the normalized Fry method (Erslev, 1988) was used on one non-recrystallized GH quartzite sample (Stop 519, Fig. 3), with 150 grains measured.

Strain analyses revealed bedding- and foliation-subparallel elongation. Elongation (R) values are shown stratigraphically on Fig. 3. Analyses on quartzite yielded lower ellipticity ratios ($R=1.2$–2.2), and on schist and phyllite revealed higher ellipticity ratios ($R=1.7$–3.1). As stated above, it is likely that strain is heterogeneous throughout the section and that significant strain may be concentrated in regions of recrystallized quartz microlithons or taken up by grain boundary sliding of micas (Holyoke and Tullis, 2006). However, in the 78 thin sections analyzed for this study we did not identify localized shear zones other than what is illustrated in Figs. 7 and 8.

To relate the strain we quantify to the top-to-the-north component of channel flow, we assume that all the strain the rocks record occurred during their exhumation path, i.e. during top-to-the-north sense deformation during channel flow, and not their burial path. We also assume that simple shear was the dominant deformation mechanism, and interpret the elongation values we obtain as shear strains. Due to the inherent challenge of capturing all strain, we used the range from the average elongation ($R=2.1$, $n=21$) to the highest observed elongation ($R=3.1$). We integrate these shear strain values over the ~11 km-thick section of the Sure transect that displays top-to-the-north shear, and regard these estimates as the permissible range for a maximum value. This suggests a total top-to-the-north component of displacement between 23 and 34 km.

5. Discussion: Implications for channel flow

5.1. Flow geometry and amount

A full Chekha Formation section in depositional contact above the GH section at Shemgang, and in fault contact across the STD at the Ura Klippe, requires the STD to cut upsection to the south. The location of this footwall ramp must lie between the southernmost exposure of the Chekha Formation in the Ura Klippe and the northernmost exposure of the Chekha Formation in the Shemgang section (Fig. 2). By projecting the northern contact at Shemgang to the east and west, we can measure the maximum north–south displacement along the STD in this location to be ~20 km (Fig. 9A).

The asymmetric channel, as defined by thin-section scale kinematic indicators in the Sure and Gonphu transects, has a top-to-the-north component of flow between 23 and 34 km (Section 4.3.4) (Fig. 9A, B). This was calculated by quantifying plastic deformation of quartz, which has lower temperature limits between 300 and 400 °C (Tullis and Yund, 1977; Kerrich et al., 1977), much lower than the 650–675 °C minimum temperatures necessary to generate significant *in situ* partial melt (Spear and Cheney, 1989), which is interpreted as critical for initiating and sustaining channel flow (Grujic, 2006;

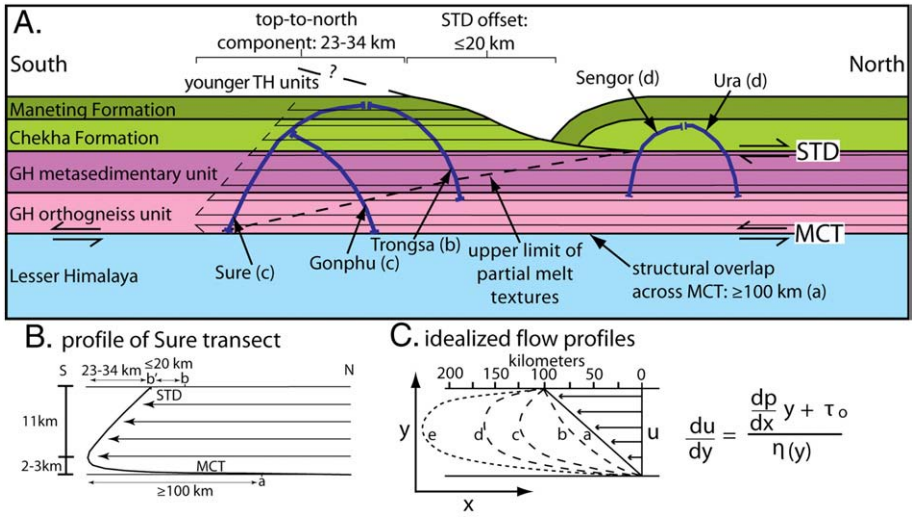

Fig. 9. A) Schematic cross-section showing structural and stratigraphic relationships observed in Shemgang and Ura areas. Levels of exposure crossed in transects shown as dark blue lines. Maximum permissible southern position of footwall ramp through Chekha Formation limits slip on STD to ~20 km. Flow lines represent schematic kinematic profile of GH channel as observed on Sure transect. Upper boundary of partial melt textures shown by dashed line. Integrated strain across channel limits top-to-north component of flow to 23–34 km. B) Cross-sectional flow profile of asymmetric channel observed on Sure transect. Asymmetric profile requires lower viscosity at base than at top. Note relative contributions from MCT overlap, STD displacement, and top-to-north component of channel flow. C) Strain profiles of idealized, uniformly-viscous channels that incorporate both shear (τ_o) and channel components; du/dy is the flow gradient, dp/dx is pressure gradient, η is viscosity. (a) 100 km of simple shear distributed across channel is based on minimum overlap across MCT (McQuarrie et al., 2008); (b) profile of channel along Trongsa transect (no top-to-north component of flow observed); (c) profile of channel along Sure transect (23–34 km top-to-north component of flow); (d) profile of channel at Ura (enough flow to localize top-to-north shear near top of GH section); (e) magnitude of flow surpasses simple shear magnitude.

Hollister and Grujic, 2006). We suggest that ductile deformation at all temperature ranges, whether melt is present or not, can contribute to flow.

Fig. 9B shows the schematic geometry of the channel at Sure, and shows that the top-to-the-north component of flow together with maximum STD offset is small compared to top-to-the-south motion, which is estimated at 100 km minimum, based on structural overlap across the MCT (McQuarrie et al., 2008). 23–34 km of top-to-the-north channel flow plus 20 km of discrete offset on the STD corresponds to only 12–15% of the 359 km of minimum shortening estimated for the Bhutan fold-thrust belt (McQuarrie et al., 2008).

We can compare our observations to idealized flow profiles, which assume a constant viscosity throughout the section (curves a–e, Fig. 9C). Top-to-the-south motion, which is at least 100 km (McQuarrie et al., 2008), is shown as distributed simple shear across the thickness of the channel (curve a). The Trongsa transect exhibits only top-to-the-south sense of shear (Fig. 3), so the top-to-the-north component of flow must not be significant compared to the magnitude of top-to-the-south simple shear there (curve b). 23–34 km of top-to-the-north shear was observed on the Sure transect (curve c), which is small compared to the top-to-the-south simple shear component. At Ura, the top-to-the-north component of flow is significant enough to localize top-to-the-north shear near the top of the GH section (curve d). Curve e illustrates a scenario where the magnitude of flow is significantly larger than the simple shear magnitude.

5.2. Variations in flow magnitude

Significant differences between the TH–GH contact that we observe near Shemgang and the contacts exposed in the Lingshi Syncline, and the Tang Chu, Ura, and Sakteng klippen (Grujic et al., 2002) are the lack of a concentrated top-to-the-north shear zone at the base of the Chekha Formation (or lower in the section), and the lack of partial melt textures through much of the GH section. The presence of melt is proposed to reduce viscosity by an order of magnitude (Beaumont et al., 2004; Rosenberg and Handy, 2005). All other factors being equal, an order of magnitude decrease in viscosity could increase flow displacement by approximately an order of magnitude. Thus if the amount of top-to-the-north flow is 23–34 km at Shemgang, flow may be as high as 230–340 km to the east and west. Since the Chekha Formation in the Ura and Tang Chu klippen has only been displaced a maximum of 20 km, to accommodate 230–340 km of channel flow, 210–320 km of flow displacement would have to be concentrated in the upper 4 km of the GH section that records a top-to-the-north sense of shear (Grujic et al., 2002).

Kellett et al. (2009) report a minimum motion age of 15.5 Ma for motion on the STD at the Lingshi Syncline and Ura Klippe, and Daniel et al. (2003) report a syn-deformational age of 22–17 Ma for the STD at the Sakteng Klippe. We obtained a 17.1 ± 0.5 Ma weighted mean age from rim analyses on an undeformed granitic partial melt body intruded into GH paragneiss just below the STD south of the Ura klippe (sample Z10B; Figs. 2 and 3, Suppl. Discussion 1, Suppl. Fig. 2B). We interpret this as the age of rim growth during granite crystallization, which constrains the minimum age of top-to-the-north shearing on the STD at Ura. Taking the above age ranges and their errors into account, the STD in eastern Bhutan could have been active from ~22 to 15.5 Ma. Assuming that channel flow occurred between 22 and 15.5 Ma, the above displacement estimates would suggest flow rates between ca. 32 and 49 mm/yr, which are many times higher than channel flow model predictions of 10 mm/yr (Beaumont et al., 2006).

In addition, if the Shemgang region acted as a viscous plug surrounded by lower-viscosity, far-traveled material, diverging flow in lower-viscosity GH rocks north of Shemgang and converging flow in the Kuru Chu Valley between the Ura and Sakteng klippen (Fig. 1) would be predicted. However, mineral stretching lineation azimuths in GH, TH and LH rocks throughout central and eastern Bhutan refute the possibility of diverging and converging flow paths (Suppl. Fig. 5). Although there is scatter (lineation azimuths diverge up to ~40° from N), a similar azimuth range is observed in both central and eastern Bhutan, and the data is approximately evenly distributed around north. This indicates that the variation in lineation azimuth is the result of processes other than transport direction variations.

A key implication of along-strike variation in viscosity and flow velocity would be long-wavelength (~100 km along-strike distance)

and large amplitude (~100–300 km in the direction of flow) variations in displacement along the MCT, which would result in salients and recessionals in map view, similar to those observed in the Zagros Range in Iran or the Sulaiman Range in Pakistan, where a weak detachment allows for rapid foreland propagation of the deformation front. Unlike more brittle structures, these lateral changes in viscosity would not require significant cross structures to accommodate differential flow. If the melt rich, potentially low-viscosity region between the Ura and Sakteng klippen (Fig. 1) experienced large magnitudes of flow, GH rock would have been emplaced on LH rocks as much as ~300 km south of its modern southern extent, or similar magnitudes of material would have to had been removed via erosion at the same time as extrusion. The metamorphic grade of Lesser Himalayan rocks exposed along the Kuru Chu valley (Fig. 1) just south of Ura and Sakteng never saw temperatures above 500 °C and many are below 300 °C (Gansser, 1983; McQuarrie et al., 2008; Long, unpublished work). Coeval motion on the MCT and STD spans ~6.5 myr in Bhutan, and if flow magnitudes as large as those discussed above occurred, erosion rates of ~30–50 mm/yr would be required to remove ~200–300 km of material over this window of time. These erosion rates are an order of magnitude higher than the 2–5 mm/yr erosion rates measured throughout the Himalaya at a variety of timescales (e.g. Galy and France-Lanord, 2001; Blythe et al., 2007; Clift et al., 2008).

6. Conclusions

Our observations at Ura, which include partial melt textures through the full GH section but not in the overlying Chekha Formation, support a top-to-the-north shear zone at the GH–TH contact, in agreement with Grujic et al. (2002). However, our observations at Shemgang, including partial melt textures only at the base of the GH section, interfingering of distinct lithologies at the GH–TH contact, and similar bioitite–muscovite–garnet mineral assemblages through the majority of the GH–TH section, indicate that TH strata are in depositional contact above GH strata. The same strata are exposed above and below the STD between Ura and Shemgang, which limits slip along the structure to ~20 km.

At Shemgang, thin-section scale kinematic indicators fit the profile of an asymmetric channel with a 2–3 km-thick section showing a top-to-the-south shear sense at the base overlain by a ~11-km-thick section showing a top-to-the-north shear sense. The lack of partial melt textures indicates that central Bhutan contains a viscous, low-grade channel when compared to GH sections studied in eastern Bhutan. Quartz recrystallization microstructure highlights a ~250–300 °C along-strike change in the temperature conditions recorded by GH rocks, and the strain recorded by plastically-elongated quartz grains integrated across the GH–TH section indicates a top-to-the-north component of channel flow between 23 and 34 km.

The preliminary data presented here beckon for future studies focused on detailed metamorphic analysis of the P–T conditions recorded by the GH and TH rocks in central Bhutan, which would serve as a rigorous test of our stratigraphic contact interpretation. The stratigraphically-continuous section proposed here, in conjunction with low offsets along a segment of the STD, has significant implications for the role of channel flow processes in orogenic development. If the dramatic along-strike gradient in metamorphic grade of the GH section that we document between eastern and central Bhutan were matched by changes in viscosity, there would be potential for significant along-strike differences in flow velocity and material transport. For erosion to keep pace with these zones of high displacement requires erosion rates much greater than those measured in the Himalaya, or even predicted by channel flow models. In addition, erosion would have to vary in space with the displacement gradients. So, we conclude that, when present, the magnitude of channel flow must be small with respect to the total mass balance of material in the system. In central Bhutan, the total top-to-the-north component of channel flow represents only 12–15% of the total amount of mass added by shortening within the Himalayan orogenic belt.

Acknowledgements

We would like to thank the government of Bhutan for their assistance and support, particularly T. Tobgay and Director General D. Wangda of the Department of Geology and Mines in the Ministry of Economic Affairs. George Gehrels and Victor Valencia of the Arizona LaserChron Center (supported by EAR-0443387 and EAR-0732436) provided assistance with U–Pb dating. This work was supported by NSF EAR 0738522 to N. McQuarrie. We are also grateful to Lincoln Hollister, Allan Rubin, Djordje Grujic and Matt Kohn for their discussions and comments, and to Mike Searle and An Yin for constructive reviews of an early version of this manuscript.

Appendix A. Supplementary data

Supplementary data associated with this article can be found, in the online version, at doi: 10.1016/j.epsl.2009.12.033.

References

Beaumont, C., Jamieson, R.A., Nguyen, M.H., Lee, B., 2001. Himalayan tectonics explained by extrusion of a low-viscosity crustal channel coupled to focused surface denudation. Nature 414, 738–742.
Beaumont, C., Jamieson, R.A., Nguyen, M.H., Medvedev, S., 2004. Crustal channel flows: 1. Numerical models with applications to the tectonics of the Himalayan–Tibetan orogen. J. Geophys. Res. 109 29 pp.
Beaumont, C., Nguyen, M.H., Jamieson, R.A., Ellis, S., 2006. Crustal flow modes in large hot orogens. In: Law, R.D., Searle, M.P., Godin, L. (Eds.), Channel Flow, Ductile Extrusion and Exhumation in Continental Collision Zones: Geol. Soc. London Spec. Pub., vol. 268, pp. 91–145.
Bhargava, O.N., 1995. The Bhutan Himalaya: a geological account. Geol. Soc. India Spec. Pub. 39 245 pp.
Blumenfeld, P., Mainprice, D., Bouchez, J.L., 1986. C-slip in quartz from subsolidus deformed granite. Tectonophysics 27, 271–294.
Blythe, A.E., Burbank, D.W., Carter, A., Schmidt, K., Putkonen, J., 2007. Plio-Quaternary exhumation history of the central Himalaya: 1. Apatite and zircon fission-track and apatite [U–Th]/He data. Tectonics 26, TC3002.
Burchfiel, B.C., Zhiliang, C., Hodges, K.V., Yuping, L., Royden, L.H., Changrong, D., Jiene, X., 1992. The south Tibetan detachment system, Himalayan orogen: extension contemporaneous with and parallel to shortening in a collisional mountain belt. Geol. Soc. Am. Spec. Paper, 269. 41 pp.
Burg, J.P., 1983. Tectogenese compare de deux segments de chaine de collision: le sud du Tibet (suture du Tsangpo), la chaine hercynienne en Europe (suture du Massif Central). Thesis, Montpellier, 450 pp.
Burg, J.P., Brunnel, M., Gapais, D., Chen, G.M., Liu, G.H., 1984. Deformation of leucogranites of the crystalline main central sheet in southern Tibet (China). J. Struct. Geol. 6, 535–542.
Cawood, P.A., Johnson, M.R.W., Nemchin, A.A., 2007. Early Paleozoic orogenesis along the Indian margin of Gondwana: tectonic response to Gondwana assembly. Earth Plan. Sci. Lett. 255, 70–84.
Clift, P.D., Hodges, K.V., Heslop, D., Hannigan, R., Van Long, H., Calves, G., 2008. Correlation of Himalayan exhumation rates and Asian monsoon intensity. Nat. Geosci. 1, 875–880.
Daniel, C.G., Hollister, L.S., Parrish, R.R., Grujic, D., 2003. Exhumation of the Main Central thrust from lower crustal depths, Eastern Bhutan Himalaya. J. Metamorph. Geol. 21, 317–334.
Davidson, C., Grujic, D.E., Hollister, L.S., Schmid, S.M., 1997. Metamorphic reactions related to decompression and synkinematic intrusion of leucogranite, High Himalayan Crystallines, Bhutan. J. Metamorph. Geol. 15, 593–612.
DeCelles, P.G., Robinson, D.M., Quade, J., Ojha, T.P., Garzione, C.N., Copeland, P., Upreti, B.N., 2001. Stratigraphy, structure, and tectonic evolution of the Himalayan fold-thrust belt in western Nepal. Tectonics 20, 487–509.
DiPietro, J.A., Pogue, K.R., 2004. Tectonostratigraphic subdivisions of the Himalaya: a view from the west. Tectonics 23, TC5001.
Edwards, M.A., Kidd, W.S.F., Jixiang, L., Yue, Y., Clark, M., 1996. Multi-stage development of the southern Tibetan detachment system near Khula Kangri; New data from Gonto La. Tectonophysics 260, 1–19.
Erslev, E.A., 1988. Normalized center-to-center analysis of packed aggregates. J. Struct. Geol. 10, 201–209.
Galy, A., France-Lanord, C., 2001. Higher erosion rates in the Himalaya: geochemical constraints on riverine fluxes. Geology 29, 23–26.
Gansser, A., 1964. Geology of the Himalayas. Wiley-Interscience, New York. 289 pp.
Gansser, A., 1983. Geology of the Bhutan Himalaya. Birkhauser Verlag, Boston. 181 pp.

Gehrels, G.E., DeCelles, P.G., Martin, A., Ojha, T.P., Pinhassi, G., 2003. Initiation of the Himalayan Orogen as an early Paleozoic thin-skinned thrust belt. GSA Today 13, 4–9.
Grujic, D., 2006. Channel flow and continental collision tectonics: an overview. In: Law, R.D., Searle, M.P., Godin, L. (Eds.), Channel Flow, Ductile Extrusion and Exhumation in Continental Collision Zones: Geol. Soc. London Spec. Pub., vol. 268, pp. 25–37.
Grujic, D., Casey, M., Davidson, C., Hollister, L.S., Kundig, R., Pavlis, T., Schmid, S., 1996. Ductile extrusion of the Higher Himalayan Crystallines in Bhutan: evidence from quartz microfabrics. Tectonophysics 260, 21–43.
Grujic, D., Hollister, L.S., Parrish, R.R., 2002. Himalayan metamorphic sequence as an orogenic channel: insight from Bhutan. Earth Planet. Sci. Lett. 198, 177–191.
Harris, N., 2007. Channel flow and the Himalayan–Tibetan orogen: a critical review. J. Geol. Soc. (Lond.) 164, 511–523.
Harrison, T.M., 2006. Did the Himalayan Crystallines extrude partially molten from beneath the Tibetan Plateau? In: Law, R.D., Searle, M.P., Godin, L. (Eds.), Channel Flow, Ductile Extrusion and Exhumation in Continental Collision Zones: Geol. Soc. London Spec. Pub., vol. 268, pp. 237–254.
Heim, A., Gansser, A., 1939. Central Himalaya: geological observations of the Swiss expedition, 1936. Mem. Swiss Soc. Nat. Sci. 73 245 pp.
Hollister, L.S., Grujic, D., 2006. Pulsed channel flow in Bhutan. In: Law, R.D., Searle, M.P., Godin, L. (Eds.), Channel Flow, Ductile Extrusion and Exhumation in Continental Collision Zones: Geol. Soc. London Spec. Pub., vol. 268, pp. 415–423.
Holyoke, C.W., Tullis, J., 2006. Formation and maintenance of shear zones. Geology 34, 105–108.
Jamieson, R.A., Beaumont, C., Medvedev, S., Nguyen, M.H., 2004. Crustal channel flows: 2. Numerical models with implications for metamorphism in the Himalayan–Tibetan Orogen. J. Geophys. Res. 109.
Jamieson, R.A., Beaumont, C., Nguyen, M.H., Grujic, D., 2006. Provenance of the Greater Himalayan Sequence and associated rocks: predictions of channel flow models. In: Law, R.D., Searle, M.P., Godin, L. (Eds.), Channel Flow, Ductile Extrusion and Exhumation in Continental Collision Zones: Geol. Soc. London Spec. Pub., vol. 268, pp. 165–182.
Kellett, D.A., Grujic, D., Erdmann, S., 2009. Miocene structural reorganization of the South Tibetan detachment, eastern Himalaya: implications for continental collision. Lithosphere 1, 259–281. doi:10.1130/L56.1.
Kerrich, R., Beckinsale, R.D., Durham, J.J., 1977. The transition between deformation regimes dominated by intercrystalline diffusion and intracrystalline creep evaluated by oxygen isotope thermometry. Tectonophysics 38, 241–257.
Kohn, M.J., 2008. P–T–t data from central Nepal support critical taper and repudiate large-scale channel flow of the Greater Himalayan Sequence. Geol. Soc. Am. Bull. 120, 259–273.
Kruhl, J.H., 1996. Prism- and basal-plane parallel subgrain boundaries in quartz: a microstructural geothermobarometer. J. Metamorph. Geol. 14, 581–589.
LeFort, P., 1975. Himalayas: the collided range, present knowledge of the continental arc. Am. J. Sci. 275-A, 1–44.
Lister, G.S., Dornsiepen, U.F., 1982. Fabric transitions in the Saxony granulite terrain. J. Struct. Geol. 4, 81–92.
Mainprice, D.H., Bouchez, J.L., Blumenfeld, P., Tubia, J.M., 1986. Dominant c slip in naturally-deformed quartz: implications for dramatic plastic softening at high temperature. Geology 14, 819–822.
McQuarrie, N., Robinson, D., Long, S., Tobgay, T., Grujic, D., Gehrels, G., Ducea, M., 2008. Preliminary stratigraphic and structural architecture of Bhutan: implications for the along-strike architecture of the Himalayan system. Earth Planet. Sci. Lett. 272, 105–117.
Nelson, K.D., Zhao, W., Brown, L.D., Kuo, J., Che, J., Liu, X., Klemperer, S.L., Makovsky, Y., Meissner, R., Mechie, J., Kind, R., Wenzel, F., Ni, J., Nabelek, J., Chen, L., Tan, H., Wei, W., Jones, A.G., Booker, J., Unsworth, M., Kidd, W.S.F., Hauck, M., Alsdorf, D., Ross, A., Cogan, M., Wu, C., Sandvol, E., Edwards, M., 1996. Partially molten middle crust beneath southern Tibet: a synthesis of Project INDEPTH results. Science 274, 1684–1688.
Passchier, C.W., Trouw, R.A.J., 1998. Microtectonics. Springer, New York. 289 pp.
Ramsay, J.G, Huber, M.I., 1983. Techniques of Modern Structural Geology, Vol. 1: Strain Analysis. Academic Press, London, 307 pp.
Robinson, D.M., Pearson, O.N., 2006. Exhumation of Greater Himalayan rock along the Main Central Thrust in Nepal: implications for channel flow. In: Law, R.D., Searle, M.P., Godin, L. (Eds.), Channel Flow, Ductile Extrusion and Exhumation in Continental Collision Zones: Geol. Soc. London Spec. Pub., vol. 268, pp. 255–267.
Robinson, D.M., DeCelles, P.G., Copeland, P., 2006. Tectonic evolution of the Himalayan thrust belt in western Nepal: implications for channel flow models. Geol. Soc. Am. Bull. 118, 865–885.
Rosenberg, C.L., Handy, M.R., 2005. Experimental deformation of partially-melted granite revisited: implications for the continental crust. J. Metamorph. Geol. 23, 19–28.
Schmid, S.M., 1994. Textures of geological materials: computer model predictions versus empirical interpretations based on rock deformation experiments and field studies. In: Bunge, H.J., Siegesmund, S., Skrotzki, W., Weber, K. (Eds.), Textures of Geological Materials. DGM Informations-gesellschaft, Oberursel, pp. 279–302.
Searle, M.P., 1999. Extensional and compressional faults in the Everest-Lhotse massif, Khumbu Himalaya, Nepal. J. Geol. Soc. (Lond.) 156, 227–240.
Searle, M.P., Law, R.D., Jessup, M.J., 2006. Crustal structure, restoration and evolution of the Greater Himalaya in Nepal–South Tibet: implications for channel flow and ductile extrusion of the middle crust. In: Law, R.D., Searle, M.P., Godin, L. (Eds.), Channel Flow, Ductile Extrusion and Exhumation in Continental Collision Zones: Geol. Soc. London Spec. Pub., vol. 268, pp. 355–378.
Simpson, C., Wintsch, R.P., 1989. Evidence for deformation-induced K-feldspar replacement by myrmekite. J. Metamorph. Geol. 7, 261–275.
Spear, F.S., Cheney, J.T., 1989. A petrogenetic grid for pelitic schists. Contrib. Mineral. Petrol. 101, 149–164.
Spear, F.S., Kohn, M.J., Cheney, J.T., 1999. P–T paths from anatectic pelites. Contrib. Mineral. Petrol. 134, 17–32.
Stipp, M., Stunitz, H., Heilbronner, R., Schmid, S.M., 2002. The eastern Tonale fault zone: a 'natural laboratory' for crystal plastic deformation over a temperature range from 250° to 700 °C. J. Stuct. Geol. 24, 1861–1884.
Stocklin, J., and Bhattarai, K.D., 1980. Geological map of Kathmandu area and central Mahabharat Range. Ministry of Industry and Commerce, Department of Mines and Geology, Kathmandu, scale 1:250,000.
Swapp, S.M., Hollister, L.S., 1991. Inverted metamorphism within the Tibetan slab of Bhutan: evidence for a tectonically transported heat source. Can. Mineral. 29, 1019–1041.
Tangri, S.K., Pande, A.C., 1995. Tethyan sequence. In: Bhargava, O.N. (Ed.), The Bhutan Himalaya: a Geological Account: Geol. Soc. India Spec. Pub., vol. 39, pp. 109–142.
Tullis, J., Yund, R.A., 1977. Experimental deformation of dry Westerly granite. J. Geophys. Res. 82, 5705–5718.
Turcotte, D.L., Schubert, G., 2002. Geodynamics. Cambridge University Press, New York. 456 pp.
Upreti, B.N., 1999. An overview of the stratigraphy and tectonics of the Nepal Himalaya. J. Asian Earth Sci. 17, 577–606.
Voll, G., 1976. Recrystallization of quartz, biotite, and feldspars from Erstlfeld to the Leventina Nappe, Swiss Apls, and it geological significance: Schweiz. Min. Pet. Mittl. 56, 641–647.
Wadia, D.N., 1934. The Cambrian-Trias sequence of northwest Kashmir (parts of the Mazaffarabad and Baramula District). Rec. Geol. Surv. India 68, 121–146.
White, S., 1975. Tectonic deformation and recrystallization of oligoclase. Contrib. Mineral. Petrol. 50, 287–304.
Yin, A., 2006. Cenozoic tectonic evolution of the Himalayan orogen as constrained by along-strike variation of structural geometry, exhumation history, and foreland sedimentation. Earth Sci. Rev. 76, 1–131.
Yin., A., Dubey, C.S., Kelty, T.K., Webb, A.A.G., Harrison, T.M., Chou, C.Y., Celerier, J., in press. Geologic correlation of the Himalayan orogen and Indian Craton (part 2): structural geology, geochronology and tectonic evolution of the Eastern Himalaya. Geol. Soc. Am. Bull. doi:10.1130/B26460.1.